# Mercury budget in global rivers at present-day: impacts from reservoirs and dams

Dong Peng[1,2], Zeli Tan[3], Peipei Wu[4], Ruirong Chang[2], Shaojian Huang[2], Peng Zhang[2], Yujuan Wang[2], Zhengcheng Song[2], Yanxu Zhang[5], Ting Lei[6], Maodian Liu[7], Jianhua Gao[1], Junguo Liu[8], Guangchun Lei[6], Shu Tao[7,9]

[1]School of Geography and Ocean Science, Ministry of Education Key Laboratory for Coast and Island Development, Nanjing University, Nanjing, China

[2]School of Atmospheric Sciences, Nanjing University, Nanjing, China

[3]Pacific Northwest National Laboratory, Richland, WA, USA

[4]Scripps Institution of Oceanography, University of California San Diego, La Jolla, CA, USA

[5]Department of Earth and Environmental Sciences, Tulane University, New Orleans, LA, USA

[6]School of Ecology and Nature Conservation, Beijing Forestry University, Beijing, China

[7]College of Urban and Environmental Sciences, Peking University, Beijing, China

[8]Henan Provincial Key Laboratory of Hydrosphere and Watershed Water Security, North China University of Water Resources and Electric Power, Zhengzhou, China

[9]School of Environmental Science and Engineering, Southern University of Science and Technology, Shenzhen, China

*Corresponding author: Yanxu Zhang (yzhang127@tulane.edu)

Peer review status:

This is a non-peer-reviewed preprint submitted to EarthArXiv.

## Abstract

Many world rivers are currently polluted by mercury (Hg) compounds, leading to the bioaccumulation of methylmercury (MeHg) in the food web, which poses potential health risks to humans. However, the riverine Hg budgets of global scale remain poorly understood due to limited observations, complicating efficient environmental governance. Here, we employ a process-driven Hg model to track its journey from sources to the global ocean and assess its human exposure. Our findings indicate that ~1,500 Mg/yr of human-induced Hg are released plus ~400 Mg/yr (mean) of soil erosional Hg are released to rivers. Due to the trapping effects of reservoirs/dams, about 50% of the riverine Hg (~1,000 Mg/yr, mean) reaches the ocean. The different strengths of the human-induced Hg releases and/or the numbers of (mega-) reservoirs/dams in regions would greatly impacts the riverine Hg budgets of the corresponding regions. Human-induced Hg releases have led to an accumulation rate of approximately ~1,000 Mg/yr in global reservoirs at present-day levels. This has resulted in large Hg pools in reservoirs and dams, posing significant risks to future Hg pollutant restoration efforts. Our model enhances the understanding of the fate of riverine Hg, providing critical information for riverine Hg management and human health mitigation strategies.


## Introduction

River pollution by mercury (Hg), recognized as one of the most toxic heavy metals, poses significant threats to global water resources and aquatic ecosystems (Mason et al. 2012, Obrist et al. 2018, Liu et al. 2021, Peng et al. 2023). The riverine Hg budget is the vital part to the global Hg budget as the connections between the Hg pools of land and ocean (Liu et al. 2021). Significant amounts of wastewater and Hg-containing wastes have been discharged into the global rivers, leading to elevated Hg concentrations in the related streams and aquatic wildlife (Eagles-Smith et al. 2009, Driscoll et al. 2013, Schoch et al. 2014). This impairs the ability of polluted rivers to provide clean water and safe food for human consumption (Zhang et al. 2021). Environmental policies, such as the Clean Water Act, freshwater fish consumption advisories, and the Minamata Convention, have been implemented to control river Hg pollution and its impact on human health (Cain et al. 2011, Wu et al. 2022). While studies have been conducted over the past decades to monitor Hg levels in river systems (Schmeltz et al. 2011, Liu et al. 2021), our understanding of its sources, transport mechanisms, fate, and drivers at a global scale remains limited.

Mercury in rivers stems from various natural and anthropogenic sources, including soil erosion, industrial wastewater (e.g., metal smelting and/or chlor-alkali production etc.), and artisanal and small-scale gold mining (ASGM) (Streets et al. 2019). At present, anthropogenic releases are the primary contributors to global riverine Hg (Kocman et al. 2017). However, relatively large uncertainty is associated with the existing releases inventories to rivers. For example, Kocman et al. (2017) estimated that approximately 1,000 Mg (300-1300 Mg) of anthropogenic Hg is discharged into global water systems annually, with contributions of 220 Mg from point sources, 40 Mg from the remobilization of contaminated systems, and 440 Mg from artisanal and small-scale

gold mining (ASGM). In another study, Streets et al. (2017) estimated that global Hg releases to land and water reached up to 7,280 Mg in 2010 but noted the challenge in separating releases between land and water due to a lack of data.

Riverine Hg primarily exists in the form of particulate Hg within suspended particulate matter (SPMs) in rivers (Schuster et al. 2011), with only a small fraction being dissolved when the total Hg concentration are in relatively higher level than the natural conditions (Lu et al. 1987, Kocman et al. 2010, Liu et al. 2021), thus the riverine Hg are largely influenced by the sediment fluxes (Liu et al. 2021, Peng et al. 2023). The nature sources, especially the soil erosion, serve as the important sources to the riverine Hg concentrations and fluxes (Liu et al. 2020), and showing impacts to the Hg concentrations in the SPMs in the rivers (Kocman et al. 2010, Peng et al. 2023). Human activities, particularly water management practices, profoundly impact the processes governing riverine Hg transport in contemporary times, especially through the construction of reservoirs and dams at a global scale. Reservoirs have substantial efficacy in trapping SPMs (Vörösmarty et al. 2003), leading to the potential sedimentation of riverine Hg. For example, the Three Gorges Dam in China has resulted in the settling of 100-200 Mg of riverine Hg in the bedload (Peng et al. 2023) and has reduced the downstream flux of riverine Hg by more than 70% (Liu et al. 2020). However, the overall impact of reservoirs and dams on river Hg transport at a global scale remains unknown.

Here, we develop a process-based global Hg model (MOSART-Hg-wrm) based on the MOdel for Scale Adaptive River Transport (with water management module, MOSART-wrm) included in the Community Earth System Model (CESM2) to simulate the transport and fate of Hg in global rivers at present-day (Peng et al. Under Review). We consider different release scenarios to bracket the uncertainty of the emission inventories and to quantify the response of river Hg levels to different emission sources. The MOSART-Hg-wrm model accounts for soil Hg erosion, the transport of Hg, and its sedimentation within river systems and corresponding watersheds (Peng et al. Under Review). We develop a new model capacity to track the trapping effect of reservoirs and dam systems on Hg based on the MOSART water management module (wrm) (Zhou et al. 2020). The riverine Hg observation records reported in the literature are used to evaluate the model results. Our objectives are (1) to develop a riverine Hg model at the present-day with human-induced releases and effects of reservoirs/dams; (2) to comprehensively understand the processes governing the transport of Hg from its sources to sinks (such as oceans and terrestrial lakes); and (3) to identify the accumulation rate of the Hg pools in the global reservoirs/dams.

## The global riverine Hg budget

Our modeling effort results in a global budget of riverine Hg, including its sources, transport, and fate (Fig. 1). Anthropogenic Hg releases approximately 7,300 Mg/yr (mean) into land and water (Streets et al. 2017), with about 20% of these entering rivers by our simulation, translating to roughly 1,500 (mean, range from 1,100-2,000) Mg/yr entering river systems. Of these human-induced Hg releases to rivers, 30%-47% originate from ASGM. The gross Hg inputs to rivers, consisting of erosional and human-induced Hg releases, total

approximately 1,900 Mg/yr, with around 30% of this amount contributed by erosional soil Hg fluxes (~400 Mg/yr).

Besides, Atmospheric Hg deposition has limited short-term impacts on erosional Hg fluxes through changes in soil Hg concentration in the watershed, indirectly increasing erosional Hg by increasing soil Hg by time (see Uncertainty analysis, *Deposition Experiment*). The long-term impacts of atmospheric Hg deposition on the watershed are accounted for in this simulation through the incorporation of soil Hg concentration changes from pre-industrial to the present-day by using the present-day soil Hg concentration dataset. Due to the barrier effect of dams and reservoirs, 40-50% of riverine Hg settles with sediments in these reservoirs. Riverine Hg from ASGM sources has a higher likelihood of reaching the oceans because reservoirs and dams predominantly align with industrial Hg sources (e.g., lower hydropower prices encourage more industrial activities).

Less than 20 Mg/yr of Hg flux is exchanged between rivers and the atmosphere due to the limited air-water exchange area of rivers. Only 110 Mg/yr of Hg sedimentation occurs in the riverbed, which could be resuspended by the wash effect from flooding pulses (mostly during wet seasons or extreme precipitation events). Ultimately, ~1,000 (777-1,146) Mg/yr of riverine Hg is exported to the ocean, with clear spatial distribution across continents, notably higher riverine Hg fluxes export to the coasts in Asia and South America than in other regions.

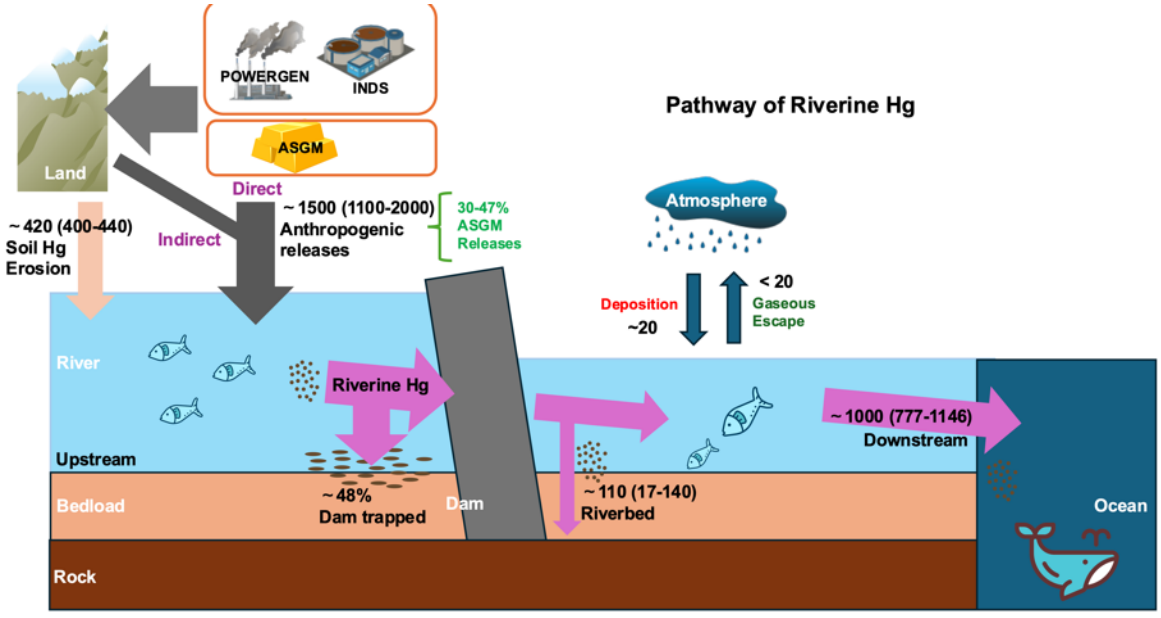


**Fig. 1 Pathways (direct and indirect) and budget** [unit: Mg/yr, mean (range)] **of Hg in global rivers**. POWERGEN = power generation, INDS = industry, ASGM = artisanal and small-scale gold mining.

## Hg inputs to the global rivers

The inputs of Hg to rivers include nature sources (soil erosion, dissolved phase Hg in water, volcano eruption etc.) and human-induced releases, with the latter as the predominant source at the present-day (Fig. 1,

2). Due to the complex of simulating the other natural sources, only soil erosion is considered in this study. We consider the *Baseline Scenario* [based on the *revised the Arctic Monitoring and Assessment Programme (AMAP) emission* scenario, see Method] wherein the gross anthropogenic Hg releases to rivers is 1,500 Mg/yr, representing the present-day conditions [with ~1,000 Mg/yr global riverine Hg budget by Liu et al. (2021)] (see Method, Table S1). We categorize anthropogenic Hg releases into two categories to align with the AMAP inventory (Steenhuisen et al. 2019, Steenhuisen et al. 2022): ***Industrial*** and ***ASGM*** (Fig. 2). The spatial distributions of anthropogenic Hg sources in North America are based on the Streets inventory (Streets et al. 2019) with other continents on the AMAP inventory (see Methods). Hence, the higher industrial Hg releases are mostly located in East Asia, South Asia, West Europe, and part of South Africa, which are align with the atmospheric Hg emissions (Fig. 2a). And the ASGM Hg releases are mostly located in South and Central America, Southeast Asia, and South-Central Africa (Fig. 2b).

The contribution of soil Hg erosion to riverine Hg is relatively small (Fig. 2c), influenced by factors such as precipitation, vegetation, soil characteristics, slope, and runoff (Dutta 2016, Peng et al. 2023, Peng et al. Under Review). In general, erosional Hg contributes 420 (400-440) Mg/yr to rivers, with a spatial distribution similar to that of the pre-industrial era (Peng et al. Under Review). Regions adjacent to plateaus, such as those near the Qinghai-Tibet Plateau in East Asia, South Asia and Southeast Asia, as well as areas near mountains, such as the west coast of South America near the Andes Mountains, show higher erosional Hg fluxes. The model also simulates significantly higher Hg erosion flux in the Amazon watershed at present-day (39.2 Mg/yr) than in the pre-industrial era (26.2 Mg/yr) due to deforestation in the region (Peng et al. Under Review). Similarly, the deforestation of the rainforest also causes higher Hg fluxes from soil erosion in Myanmar and Bangladesh (Southeast Asia) (Feinberg et al. 2024).

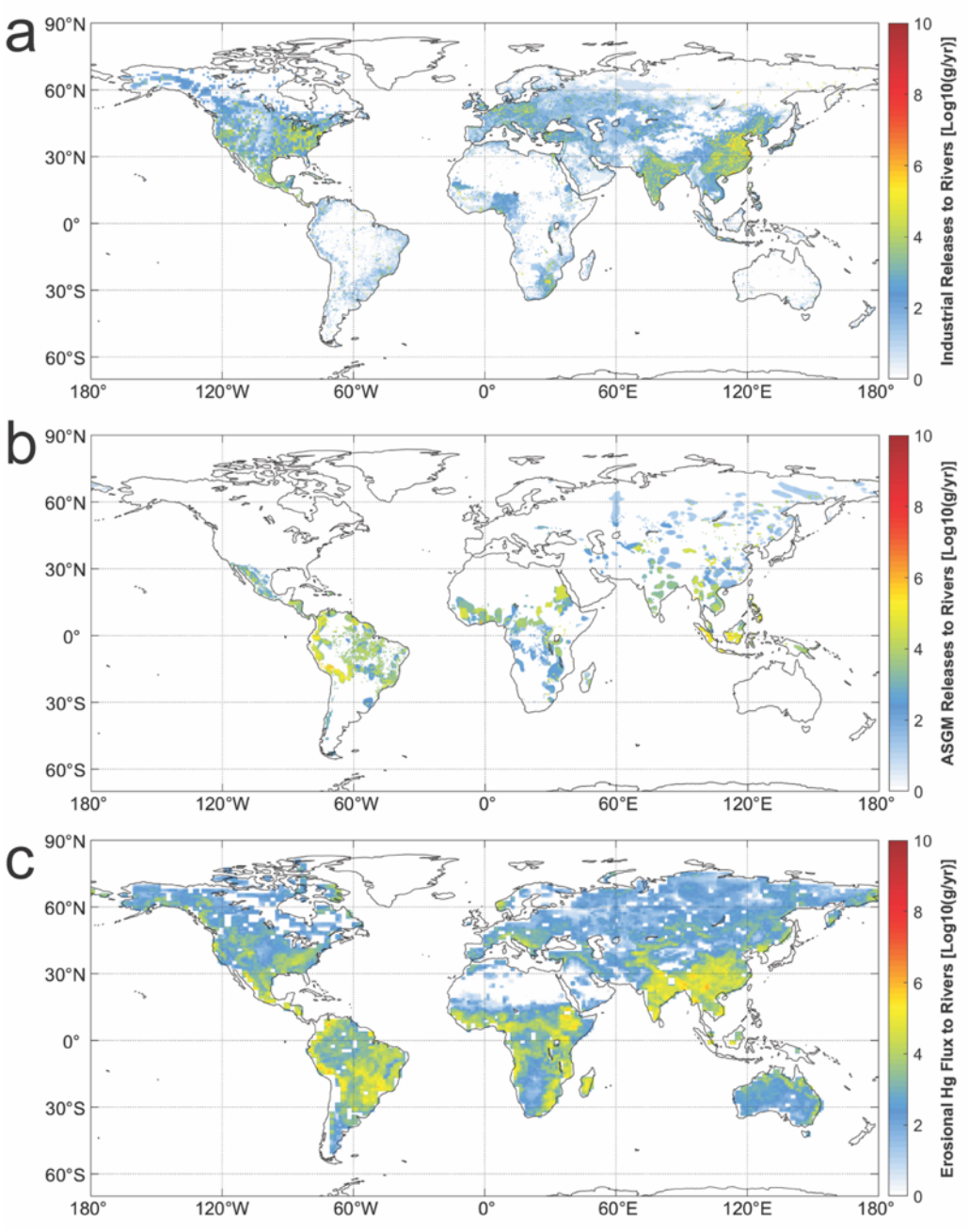


**Fig. 2 Input of Hg to global rivers**. a) Industrial releases to rivers, b) artisanal and small-scale gold mining (ASGM) releases to rivers, c) Erosional Hg flux to rivers.

## Impacts from reservoirs/dams to riverine Hg (riverine processes of Hg)

We find that reservoirs/dams can significantly influence global gross riverine Hg budget by reducing the transport flux by 40-50% (the sedimentation of riverine Hg in river channel are not included) (Fig. 1, 3). The Hg form may change after settled into the bed of reservoirs, such as methylation and/or to dissolved phase, but in this study, we assume the Hg fluxes are only impacted by resuspension at this stage due to the relatively smaller

fluxes related the biological activities and other activities (Liu et al. 2019). Water management activities, such as reservoirs and dams, play a significant role in reducing riverine Hg fluxes and SPM in downstream rivers (Syvitski et al. 2005, Syvitski et al. 2022). This is apparent in the spatial pattern of riverine Hg fluxes along channels (Fig. 2). The increasing trends of fluxes downstream can be interrupted by reservoirs and dams, which trap Hg input from upstream and decrease the flux significantly, and the fluxes continue increasing after passing the dams. We conducted paired sensitivity experiments with no water management (*Water Management Experiment*, see Method) (Table S3). The role of reservoirs and dams can be evaluated based on the differences between the paired control experiment. For example, one paired model run includes *No Human-induced Hg Release with and without Reservoir or NHHR w/wt R.* The other paired model run includes *Baseline Hg-induced Hg Releases with and without Reservoir or BHHR w/wt R* (Fig. 3).

The fluxes of riverine Hg delivery to the ocean are decreased by 41% from 417 Mg/yr (*NHHR wt R*) to 248 Mg/yr (*NHHR w R*). If we consider the anthropogenic Hg releases, reservoirs/dams reduce Hg fluxes to ocean by 50% from 2,021 Mg/yr (*BHHR wt R*) to 1,014 Mg/yr (*BHHR w R*). The difference between the two pairs of model runs reflect the large spatial variabilities in the impact of reservoirs (Fig. 3bd). For the setting with baseline anthropogenic Hg release, the riverine Hg exports of Yangtze, Yellow, Parana, and Niger River have been reduced by 77%, 75%, 63% and 61%, respectively. This variability in reduction largely reflects the number of reservoirs or/and the portion of mega reservoirs along these rivers. Indeed, some rivers show limited impacts from water management due to less reservoirs and/or less mega reservoirs along the river, such as Congo, Amazon, and Ganges-Brahmaputra River, which have been reduced by only <1%, 1%, and 17%, respectively. As for the no human-induced Hg release scenarios, the pattern is similarly to the above (Fig. 3bd).

Reservoirs regulate river flooding and consequently the seasonal fluctuations of Hg fluxes, even though human-induced Hg releases to rivers are constant across different seasons in the estimations. For example, flood pulses driven by increased runoff and larger soil erosional fluxes during the wet season contrast with reduced fluxes during the dry season, thereby altering soil Hg erosion fluxes. The differences between monthly global Hg exports have been reduced from 22.0-52.5 Mg/month (*NHHR wt R*) to 12.5-29.3 Mg/month (*NHHR w R*) with the amplitude reduced by 45% from 30.6 to 16.8 Mg/month. The monthly Hg export also decreased from 150.3-196.6 to 74.6-94.3 Mg/month under the *BHHR w/wt R* with amplitude reduced by 58% from 46.3 to 19.7 Mg/month. The damping effects of dams are more pronounced in the Northern Hemisphere (Fig. 3ef), attributed to the larger landmass, and numbers of rivers and reservoirs as compare to the Southern Hemisphere (Lehner et al. 2011, Mulligan et al. 2020). Furthermore, this effect is amplified by the larger anthropogenic Hg releases, leading to significant differences in riverine Hg fluxes during summer in the Northern Hemisphere (Fig. 3e). In conclusion, the reservoirs/dams shrink the seasonal changes of riverine Hg.

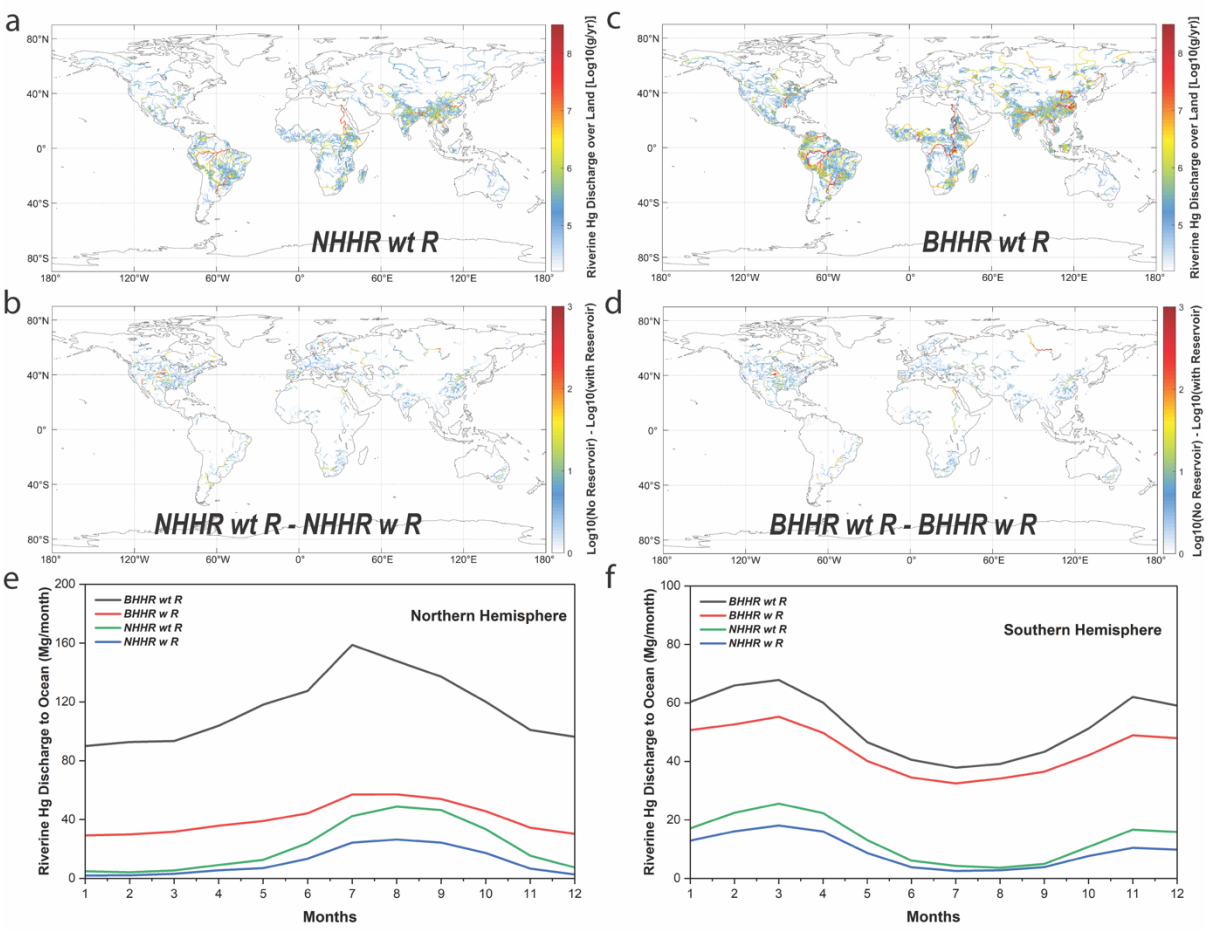


**Fig. 3 Impact of reservoir and dams on riverine Hg transport.** a) Riverine Hg fluxes in global rivers under *No Human-induced Hg Release without Reservoir scenario (NHHR wt R)*, b) Differences of riverine Hg fluxes between *No Human-induced Hg Release with/without Reservoir (NHHR w/wt R)*, c) Riverine Hg fluxes in global rivers under *Baseline Human-induced Hg Releases without Reservoir scenario (BHHR wt R)*, d) Differences of riverine Hg fluxes between *Baseline Human-induced Hg Releases with/without Reservoir (BHHR w/wt R)*, e) Monthly riverine Hg fluxes to ocean in Northern Hemisphere, f) Monthly riverine Hg fluxes to ocean in Southern Hemisphere.

## River Hg fluxes and budgets

The modeled global riverine Hg discharge to the ocean/lakes amounts to ~1,000 Mg/yr in *Baseline scenario (also the BHHR w R)* (Fig. 1, 2). The top ten largest riverine Hg exporters contribute 51% (506 Mg/yr) of the global discharge, with the highest river as the Amazon (202 Mg/yr), followed by the Congo (87 Mg/yr), Yangtze (52 Mg/yr), and Ganges-Brahmaputra (51 Mg/yr). These large rivers dwarf the export from smaller rivers in these regions (less than 30 Mg/yr), especially the smaller ones along the north coast of South America, the Indian Peninsula, the eastern China, and Southeast Asia. The denser river networks in East Asia, South America, and Central Africa could result in higher riverine Hg fluxes due to the intersection of the rivers within the large watershed. For example, the Ganges River and the Brahmaputra River share the same estuary.

The modeled riverine Hg fluxes exhibit large spatial variations and seasonal variabilities (Fig. 4 and S1). Generally, the flux of Hg in the most river increases downstream along the channel, reaching its maximum at the river mouths, if there are no major dams. This pattern reflects the continuous input of Hg from wastewater and soil erosion in their watersheds and the high transport efficacy of SPM by rivers (Peng et al. 2024). For example, the riverine Hg fluxes keep increasing in the upstream of Three Gorges Dam (0-24 Mg/yr) and this trend resume after Three Gorges Dam in the channels of Yangtze River (4-52 Mg/yr) (Fig.2). The rivers like Panama and Mekong River with increased riverine Hg fluxes along the channels and reach maximum at the river mouth, while this trend is less influenced by dams.

Rivers with higher anthropogenic releases and/or erosion in their watersheds can easily maintain higher Hg fluxes in their channels, such as the Amazon, Congo, Yangtze, and Ganges-Brahmaputra Rivers (Fig. 2 and 4). For example, the highest riverine Hg flux in the Amazon River (201.7 Mg/yr near its mouth) is caused by the effect of ASGM releases and erosional Hg flux to the watershed (152.5 and 32.2 Mg/yr, respectively). Similar situation applies to the Congo River. In contrast, the higher riverine Hg fluxes of Yangtze (52 Mg/yr at mouth) and Ganges-Brahmaputra River (51.2 Mg/yr at mouth) are caused by the higher industrial releases (100.7 and 37.8 Mg/yr, respectively) and erosional Hg flux (from Himalaya to ocean; 23.6 and 49.6 Mg/yr. respectively) in these regions. Indeed, the watersheds of these rivers include the most industrialized regions in eastern China (Fig. 2a). Interestingly, some smaller rivers with relatively small watersheds, such as Kapuas River (14.6 Mg/yr at mouth), could also have relatively higher riverine Hg fluxes due to their intense anthropogenic Hg releases (Baiq 2018).

The riverine Hg fluxes estimated by model agree well with the observation of Hg levels in river mouths (Fig. 4b). The observational dataset includes 44 rivers from different continents spanning five orders magnitudes with a geo mean flux of $1\times10^{3.99\pm3.9}$ kg/yr. The model ($19\times10^{3.90\pm3.7}$ kg/yr) reproduces the observations with a high coefficient of determination ($R^2 = 0.97$, $p<0.01$). The model results agree well with observation records for many major rivers, such as Yangtze (model vs. observation: 52 vs. 48 Mg/yr), Ob' (3.2 vs. 2.4 Mg/yr), and Hudson (0.3 vs. 0.33 Mg/yr). Although the model has performed well in simulating erosion of small rivers (Tan et al. 2022), due to the coarse anthropogenic releases the model has higher bias for smaller rivers, such as Kolyma (model vs. observation: 4.7 vs. 1.1 Mg/yr), Mackenzie (2.6 vs. 0.6 Mg/yr) and Yukon (3.8 vs. 0.9 Mg/yr). These rivers exhibit relatively lower riverine Hg fluxes compared to larger rivers, and they appear to be much more sensitive to the local anthropogenic Hg releases. For instance, discrepancies in releases in large watersheds may be mitigated by the canceling effect among grids with the same watershed, but such effect is less likely to occur in smaller watersheds. Furthermore, the model agrees with observations taken along the river channels, which is available for a few major rivers. For example, the model (24 Mg/yr) closely resembles the observation (26 Mg/yr) upstream of the Three Gorges Dam (TGD), as it does at the immediate downstream of the TGD (4.7 and 4.4 Mg/yr) (Liu et al. 2020).

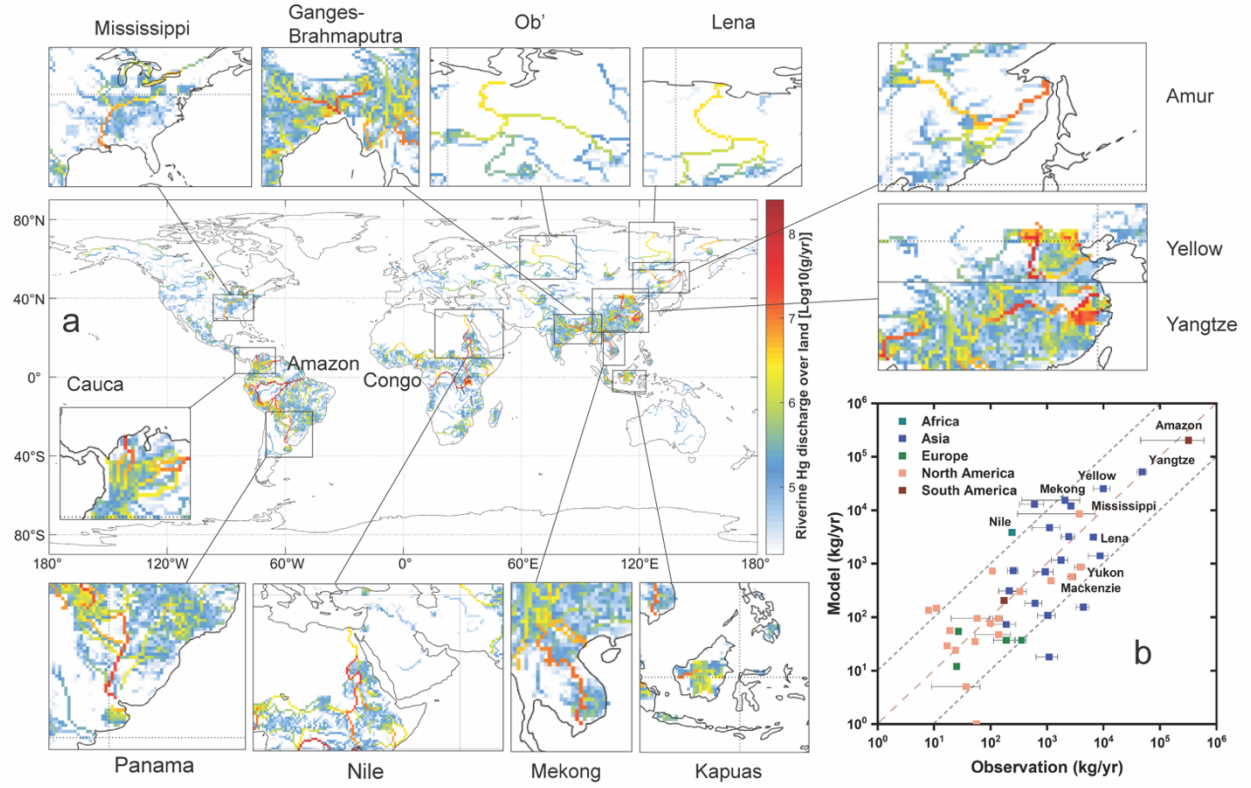


**Fig. 4 Riverine Hg fluxes in global rivers**. a) Spatial patterns with zoomed regions of major rivers; b) Model results versus observation records in continents.

## Impacts of Human-induced Hg Releases

We consider five scenarios to cover the uncertainty of anthropogenic Hg releases from industrial and ASGM sources to the rivers at present-day: (1) *Low Release* (1,100 Mg/yr), (2) *Moderate Release* (1,500 Mg/yr) (similar level with *Baseline Scenario*), (3) *High Industrial Release* (2,000 Mg/yr, ASGM contribute 600 Mg/yr), (4) *High ASGM Release* (2,000 Mg/yr, ASGM contribute 850 Mg/yr), (5) *No Release* (0 Mg/yr) (Fig. 1, 5, Table S1). The *Low Release scenario* represents the unique period during the COVID-19 pandemic when industrial and ASGM releases are significantly reduced due to lockdown measures (Wu et al. 2021) (Fig. 5a). The *Moderate Release scenario* depicts a more realistic post-Minamata Convention scenario with reduced anthropogenic Hg releases (Liu et al. 2021) (Fig. 5b). The *High Industrial Release scenario* mirror the condition around the year 2000, with relatively higher fraction of wastewater as mismanaged (Amos et al. 2014) (Fig. 5c). The *High ASGM Release scenario* represents the early phase of the Minamata Convention, when the industrial releases declined rapidly but the ASGM was still growing due to poor environmental management in the mining countries (Cheng et al. 2022, Prescott et al. 2022, Peng et al. 2023) (Fig. 5d). The *No Release scenario* is an idealized scenario with only natural sources at present-day. The different sectors contributions of Hg sources among scenarios also facilitate an assessment of the sensitivity of riverine Hg to anthropogenic releases.

The results indicate that the anthropogenic Hg releases have a significant impact on the dynamics of riverine

Hg (Fig. 5e-g). The input of Hg to rivers is increased by higher anthropogenic Hg releases, while the contribution of soil erosion remains stable under different scenarios. The fate of anthropogenic Hg releases, including riverine inputs and exports to ocean, also varies among scenarios. For instance, despite comparable levels of total releases between *High Industrial Release* and *High ASGM Release scenarios*, the former exhibits a lower export fraction (Fig. 5f). With the *Moderate Release scenario* as a reference, only 28% of the increased industrial releases are ultimately transported to the ocean for the *High Industrial Release* scenario (Table S2), but 54% exported for the *High ASGM Release scenario*.

Higher industrial releases contribute to elevated riverine budgets in rivers of East Asia and Southeast Asia, while increased ASGM releases notably amplify riverine Hg budgets in the Amazon River Watershed, Central Africa, and Southeast Asia. This is attributed to the difference of water management among regions. For instance, the Amazon River, with active ASGM activities in its watershed, has fewer reservoirs/dams and/or fewer mega reservoirs/dams, and subsequently higher export fractions. In contrast, the Yangtze River has higher industrial releases in its watershed and impact from reservoirs and dams (Fig. 3b). Indeed, regions with thriving industries often implement more extensive water management practices to provide water and hydroelectricity for reservoirs (Chen et al. 2016). This shift in water management could result in lower riverine Hg export fractions of industrial releases (Fig. 5g).

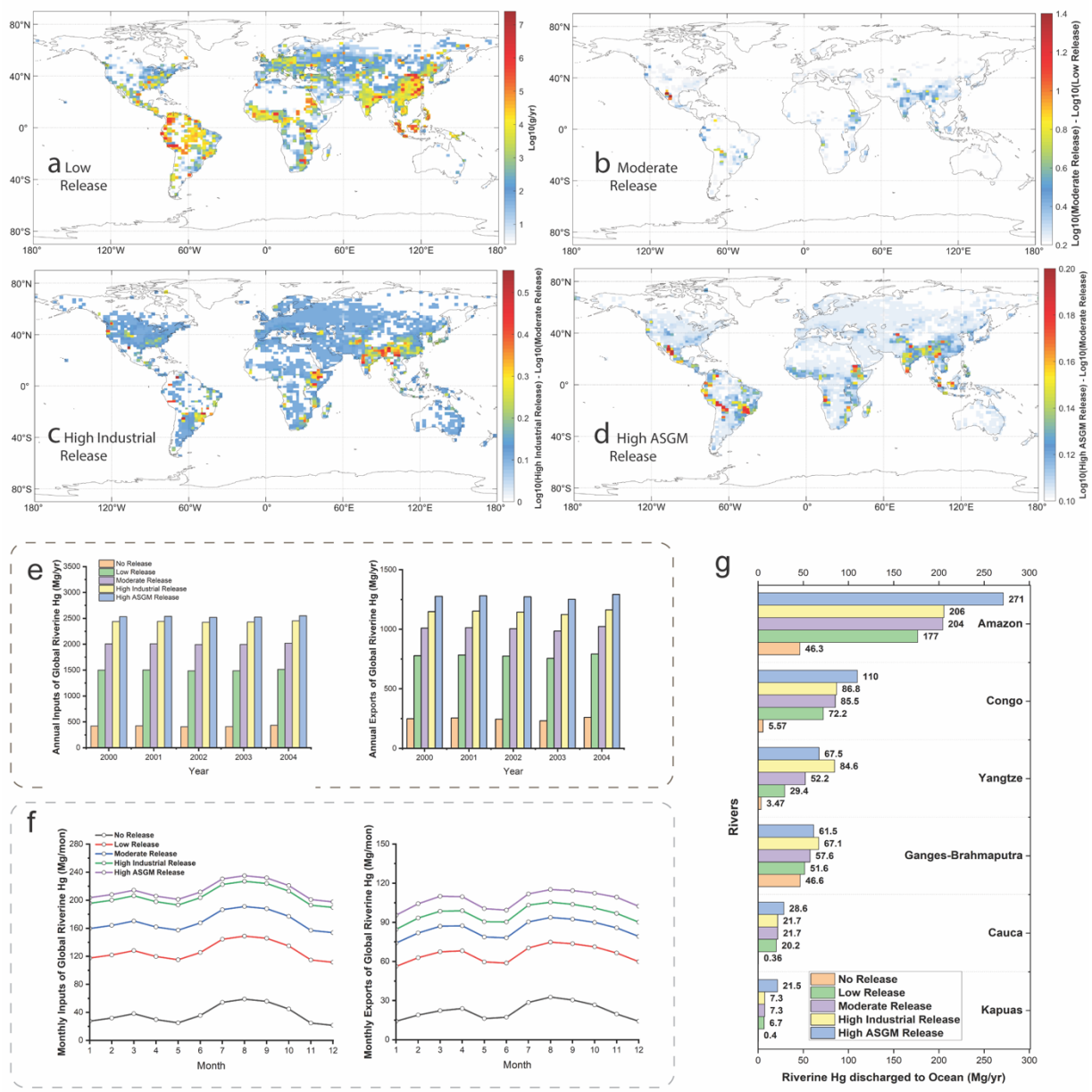


**Fig. 5 Impacts of river Hg budget associated with anthropogenic Hg releases to rivers.** a-d) Anthropogenic Hg releases under different release scenarios, e) Annual inputs and exports in global rivers under different release scenarios, f) Monthly inputs and exports in global rivers under different release scenarios, g) Riverine Hg discharges to the ocean in selected rivers under different release scenarios.

## Sink of Hg in Reservoirs/Dams

Increased Hg releases from human activities lead to higher Hg accumulation rates in reservoirs, the major sink for riverine Hg (Fig. 6). Globally, Hg accumulation rates in reservoirs rise approximately 6-fold from 14 Mg/month in the *No Release scenario* (representing pre-industrial era) to 84 Mg/month in the *Baseline Release scenario* (representing present-day). The contribution of different sectors (e.g., industrial vs. ASGM sources) to

Hg releases has a smaller effect on accumulation rates compared to riverine Hg fluxes, as shown by similar rates in the *High Industrial Release* (106 Mg/month) and *High ASGM Release* (104 Mg/month) scenarios (Fig 6a). Due to the dominance of human-induced releases over natural sources, the overall increase in accumulation shows no apparent seasonal variation, remaining relatively consistent month to month (Fig. 6a).

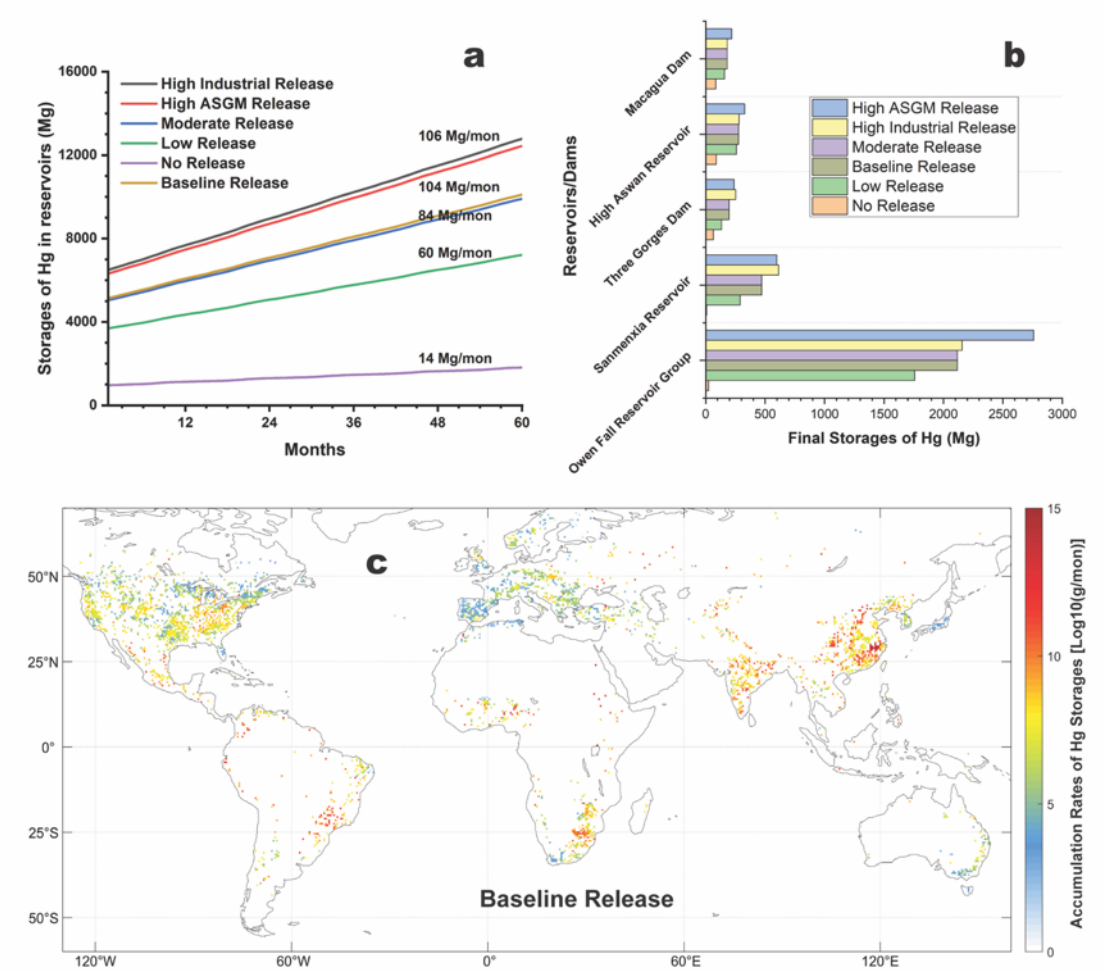


**Fig. 6 Reservoir storages of riverine Hg.** a) Storage and monthly accumulation (Mg/mon) of Hg in global reservoirs, b) final storages of Hg during 10 years of simulation in large reservoirs/dams, c) monthly accumulation rates (Mg/mon) of Hg storages in global reservoirs/dams under *Baseline Release Scenario*.

Reservoirs exhibit significant regional variabilities in the rates of Hg accumulation, influenced by reservoir density and watershed Hg releases (Fig. 6c). In East and South Asia, higher reservoir densities combined with substantial industrial Hg releases (Fig. 5) result in elevated Hg accumulation rates. In contrast, the US, despite its high reservoir density, has relatively lower Hg releases, leading to low to moderate accumulation rates. Reservoirs in parts of South Africa and South America exhibit high accumulation rates, consistent with elevated Hg releases from ASGM activities (Fig. 5). Meanwhile, Southern Europe, with a a high density of reservoirs but lower regional Hg releases, shows relatively lower Hg accumulation rates.

Several specific reservoirs illustrate the dominance of human-induced Hg releases on accumulation patterns.

For example, the Owen Falls Reservoir Group (upstream of the Nile), the High Aswan Dam (Nile), the Sanmenxia Reservoir (Yellow River), the Three Gorges Dam (Yangtze River), and the Macagua Dam (Caroní River) show substantial increases in Hg accumulation between *No Release* to *Low Release* scenarios, with even larger increases from *Low* to *Moderate* or *High Release* levels (Fig. 6b). Sectoral contributions also play a critical role: while reservoirs like the Sanmenxia and the Three Gorges experience greater accumulation under the *High Industrial Release* scenario, those such as the Owen Falls Reservoir Group see much higher accumulation rates under *High ASGM Release* scenario than the *High Industrial Release* one.

## Implications

Anthropogenic Hg releases significantly augment riverine Hg delivery from upstream to downstream and export into inland lakes and/or oceans (Liu et al. 2021, Yu et al. 2021). However, measuring riverine Hg fluxes is challenging due to rapid changes in runoff parameters and considerable variability in Hg concentrations. The lack of historical data also hinders the proper evaluation of the trends of riverine Hg export and the contribution of anthropogenic Hg releases, posing management challenges, particularly in international rivers such as the Mekong, Jordan, Indus, Niger, and Nile Rivers (Campbell 2007, Campbell 2009). Our estimation provides insights into understanding the regional-based contribution of anthropogenic Hg releases to downstream rivers and oceans. The Hg concentrations in the rivers have strong connection with the fish Hg (Scudder et al. 2009, Blanchfield et al. 2021), hence this simulation could help understand the Hg pollution status in the rivers and coastal environment, which is vital for fishing and aquaculture. Furthermore, the settled Hg in reservoirs creates a suitable environment for Hg methylation, with conditions similar to nutrient-rich wetlands that support biological activity and methylation. Our results provide valuable insights for future studies to better understand the amounts and changes of Hg pools in reservoirs, which are important for estimating and observing the methylation in the reservoirs.

Our assessments emphasize the critical role of reservoirs as significant reservoirs in global Hg biogeochemistry, despite the uncertainty surrounding their masses. The presence of settled Hg pools within global reservoirs introduces complexities to ongoing environmental governance efforts on a global scale. Although water management benefits agriculture and related industries, Hg settled in reservoir bottoms and riverbeds could potentially act as potential Hg sources to rivers (Liu et al. 2020, Peng et al. 2023). For instance, the observation in Yangtze River noticed that the settled Hg pool of the Three Gorges Dam shift from sink to the sources of riverine Hg response to the decreased riverine Hg fluxes from upstream and tributaries (Peng et al. 2023). Our model serves as a scientific tool to guide riverine Hg management strategies and identify effective pathways for reducing Hg releases, especially those impacting human health. Furthermore, our estimation of accumulation rates in global reservoirs can aid in monitoring Hg pools during restoration projects and in identifying potential risks associated with reservoir or dam management such as reservoirs/dams demolition.

## References


1 Amos, H. M., D. J. Jacob, D. Kocman, H. M. Horowitz, Y. Zhang, S. Dutkiewicz, M. Horvat, E. S. Corbitt, D. P. Krabbenhoft and E. M. Sunderland (2014). Global biogeochemical implications of mercury discharges from rivers and sediment burial. Environmental Science and Technology 48(16): 9514-9522. http://dx.doi.org/10.1021/es502134t

2 Baiq, D. K. (2018). ASGM status in West Nusa Tenggara Province, Indonesia. Journal of Degraded and Mining Lands Management 5(2): 1077.

3 Cain, A., J. T. Morgan and N. Brooks (2011). Mercury policy in the Great Lakes states: past successes and future opportunities. Ecotoxicology 20(7): 1500-1511. http://dx.doi.org/10.1007/s10646-011-0764-4

4 Campbell, I. (2009). The Challenges for Mekong River Management. The Mekong**:** 403-419. http://dx.doi.org/10.1016/b978-0-12-374026-7.00017-6

5 Campbell, I. C. (2007). Perceptions, data, and river management: Lessons from the Mekong River. Water Resources Research 43(2). http://dx.doi.org/10.1029/2006wr005130

6 Chen, J., H. Shi, B. Sivakumar and M. R. Peart (2016). Population, water, food, energy and dams. Renewable and Sustainable Energy Reviews 56: 18-28. http://dx.doi.org/10.1016/j.rser.2015.11.043

7 Cheng, Y., K. Nakajima, K. Nansai, J. Seccatore, M. M. Veiga and M. Takaoka (2022). Examining the inconsistency of mercury flow in post-Minamata Convention global trade concerning artisanal and small-scale gold mining activity. Resources, Conservation and Recycling 185. http://dx.doi.org/10.1016/j.resconrec.2022.106461

8 Driscoll, C. T., R. P. Mason, H. M. Chan, D. J. Jacob and N. Pirrone (2013). Mercury as a Global Pollutant: Sources, Pathways, and Effects. Environmental Science & Technology 47(10): 4967-4983. http://dx.doi.org/10.1021/es305071v

9 Dutta, S. (2016). Soil erosion, sediment yield and sedimentation of reservoir: a review. Modeling Earth Systems and Environment 2(3): 123. http://dx.doi.org/10.1007/s40808-016-0182-y

10 Eagles-Smith, C. A., J. T. Ackerman, S. E. De La Cruz and J. Y. Takekawa (2009). Mercury bioaccumulation and risk to three waterbird foraging guilds is influenced by foraging ecology and breeding stage. Environ Pollut 157(7): 1993-2002. http://dx.doi.org/10.1016/j.envpol.2009.03.030

11 Feinberg, A., M. Jiskra, P. Borrelli, J. Biswakarma and N. E. Selin (2024). Deforestation as an Anthropogenic Driver of Mercury Pollution. Environmental Science & Technology. http://dx.doi.org/10.1021/acs.est.3c07851

12 Kocman, D., S. Wilson, H. Amos, K. Telmer, F. Steenhuisen, E. Sunderland, R. Mason, P. Outridge and M. Horvat (2017). Toward an Assessment of the Global Inventory of Present-Day Mercury Releases to Freshwater Environments. International Journal of Environmental Research and Public Health 14(2): 138. http://dx.doi.org/10.3390/ijerph14020138

13 Lehner, B., C. R. Liermann, C. Revenga, C. Vörösmarty, B. Fekete, P. Crouzet, P. Döll, M. Endejan, K. Frenken, J. Magome, C. Nilsson, J. C. Robertson, R. Rödel, N. Sindorf and D. Wisser (2011). High-resolution mapping of the world's reservoirs and dams for sustainable river-flow management. Frontiers in Ecology and the Environment 9(9): 494-502. http://dx.doi.org/10.1890/100125

14 Liu, M., Y. He, Z. Baumann, Q. Zhang, X. Jing, R. P. Mason, H. Xie, H. Shen, L. Chen, W. Zhang, Q. Zhang and X. Wang (2020). The impact of the Three Gorges Dam on the fate of metal contaminants across the river-ocean continuum. Water Research 185: 116295. http://dx.doi.org/10.1016/j.watres.2020.116295

15 Liu, M., Q. Zhang, T. Maavara, S. Liu, X. Wang and P. A. Raymond (2021). Rivers as the largest source of mercury to coastal oceans worldwide. Nature Geoscience 14(9): 672-677. http://dx.doi.org/10.1038/s41561-021-00793-2

16 Liu, M., Q. Zhang, C. Yu, L. Yuan, Y. He, W. Xiao, H. Zhang, J. Guo, W. Zhang, Y. Li, Q. Zhang, L. Chen and X. Wang (2021). Observation-Based Mercury Export from Rivers to Coastal Oceans in East Asia. Environmental Science & Technology 55(20): 14269-14280. http://dx.doi.org/10.1021/acs.est.1c03755

17 Mason, R. P., A. L. Choi, W. F. Fitzgerald, C. R. Hammerschmidt, C. H. Lamborg, A. L. Soerensen and E. M. Sunderland (2012). Mercury biogeochemical cycling in the ocean and policy implications. Environmental Research 119: 101-117. http://dx.doi.org/10.1016/j.envres.2012.03.013

18 Mulligan, M., A. van Soesbergen and L. Sáenz (2020). GOODD, a global dataset of more than 38,000 georeferenced dams. Scientific Data 7(1). http://dx.doi.org/10.1038/s41597-020-0362-5

19 Obrist, D., J. L. Kirk, L. Zhang, E. M. Sunderland, M. Jiskra and N. E. Selin (2018). A review of global environmental mercury processes in response to human and natural perturbations: Changes of emissions, climate, and land use. Ambio 47(2): 116-140. http://dx.doi.org/10.1007/s13280-017-1004-9

20 Peng, D., J. Lyu, Z. Song, S. Huang, P. Zhang, J. Gao and Y. Zhang (2023). Mercury budgets in the suspended particulate matters of the Yangtze River. Water Research 243. http://dx.doi.org/10.1016/j.watres.2023.120390

21 Peng, D., Z. Tan, T. Yuan, P. Wu, Z. Song, P. Zhang, S. Huang, Y. Zhang, T. Lei, B. A. Middleton, G. Lei and J. Gao (Under Review). Human perturbations to mercury in global rivers.

22 Prescott, G. W., M. Baird, S. Geenen, B. Nkuba, J. Phelps and E. L. Webb (2022). Formalizing artisanal and small-scale gold mining: A grand challenge of the Minamata Convention. One Earth 5(3): 242-251. http://dx.doi.org/10.1016/j.oneear.2022.02.005

23 Schmeltz, D., D. C. Evers, C. T. Driscoll, R. Artz, M. Cohen, D. Gay, R. Haeuber, D. P. Krabbenhoft, R. Mason, K. Morris and J. G. Wiener (2011). MercNet: a national monitoring network to assess responses to changing mercury emissions in the United States. Ecotoxicology 20(7): 1713-1725. http://dx.doi.org/10.1007/s10646-011-0756-4

24 Schoch, N., M. J. Glennon, D. C. Evers, M. Duron, A. K. Jackson, C. T. Driscoll, J. W. Ozard and A. K. Sauer (2014).

The Impact of Mercury Exposure on the Common Loon (Gavia immer) Population in the Adirondack Park, New York, USA. Waterbirds 37: 133-146. http://dx.doi.org/10.1675/063.037.sp116

25 Schuster, P. F., R. G. Striegl, G. R. Aiken, D. P. Krabbenhoft, J. F. Dewild, K. Butler, B. Kamark and M. Dornblaser (2011). Mercury Export from the Yukon River Basin and Potential Response to a Changing Climate. Environmental Science & Technology 45(21): 9262-9267. http://dx.doi.org/10.1021/es202068b

26 Steenhuisen, F. and S. J. Wilson (2019). Development and application of an updated geospatial distribution model for gridding 2015 global mercury emissions. Atmospheric Environment 211: 138-150. http://dx.doi.org/10.1016/j.atmosenv.2019.05.003

27 Steenhuisen, F. and S. J. Wilson (2022). Geospatially distributed (gridded) global mercury emissions to air from anthropogenic sources in 2015, DataverseNL.

28 Streets, D. G., H. M. Horowitz, D. J. Jacob, Z. Lu, L. Levin, A. F. H. ter Schure and E. M. Sunderland (2017). Total Mercury Released to the Environment by Human Activities. Environmental Science & Technology 51(11): 5969-5977. http://dx.doi.org/10.1021/acs.est.7b00451

29 Streets, D. G., H. M. Horowitz, Z. Lu, L. Levin, C. P. Thackray and E. M. Sunderland (2019). Five hundred years of anthropogenic mercury: spatial and temporal release profiles*. Environmental Research Letters 14(8). http://dx.doi.org/10.1088/1748-9326/ab281f

30 Streets, D. G., H. M. Horowitz, Z. Lu, L. Levin, C. P. Thackray and E. M. Sunderland (2019). Global and regional trends in mercury emissions and concentrations, 2010–2015. Atmospheric Environment 201: 417-427. http://dx.doi.org/10.1016/j.atmosenv.2018.12.031

31 Syvitski, J., J. R. Ángel, Y. Saito, I. Overeem, C. J. Vörösmarty, H. Wang and D. Olago (2022). Earth's sediment cycle during the Anthropocene. Nature Reviews Earth & Environment 3(3): 179-196. http://dx.doi.org/10.1038/s43017-021-00253-w

32 Syvitski, J. P., C. J. Vorosmarty, A. J. Kettner and P. Green (2005). Impact of humans on the flux of terrestrial sediment to the global coastal ocean. Science 308(5720): 376-380. http://dx.doi.org/10.1126/science.1109454

33 Tan, Z., L. R. Leung, H. Y. Li and S. Cohen (2022). Representing Global Soil Erosion and Sediment Flux in Earth System Models. Journal of Advances in Modeling Earth Systems 14(1). http://dx.doi.org/10.1029/2021ms002756

34 Vörösmarty, C. J., M. Meybeck, B. Fekete, K. Sharma, P. Green and J. P. M. Syvitski (2003). Anthropogenic sediment retention: major global impact from registered river impoundments. Global and Planetary Change 39(1-2): 169-190. http://dx.doi.org/10.1016/s0921-8181(03)00023-7

35 Wu, P. and Y. Zhang (2023). Toward a Global Model of Methylmercury Biomagnification in Marine Food Webs: Trophic Dynamics and Implications for Human Exposure. Environmental Science & Technology 57(16): 6563-6572. http://dx.doi.org/10.1021/acs.est.3c01299

36 Wu, Q., Y. Tang, L. Wang, S. Wang, D. Han, D. Ouyang, Y. Jiang, P. Xu, Z. Xue and J. Hu (2021). Impact of emission reductions and meteorology changes on atmospheric mercury concentrations during the COVID-19 lockdown. Science of The Total Environment 750. http://dx.doi.org/10.1016/j.scitotenv.2020.142323

37 Wu, Q., Y. Zhang, P. Li, X. Fu, Q. Zhang, X. Wang, L. Chen, S. Wang, F. Wang and X. Feng (2022). Ecosystem Mercury Recovery and Health Benefit Under the Minamata Convention in a Changing Climate. REVIEWS OF ENVIRONMENTAL CONTAMINATION AND TOXICOLOGY 260(1). http://dx.doi.org/10.1007/s44169-022-00016-8

38 Yu, C. H., Y. P. Xu, Y. Y. Yan, W. J. Xiao, M. D. Liu, M. H. Cheng, W. He, F. L. Xu and X. J. Wang (2021). Mercury and methylmercury in China's lake sediments and first estimation of mercury burial fluxes. Science of the Total Environment 770. http://dx.doi.org/10.1016/j.scitotenv.2021.145338

39 Zhang, Y., Z. Song, S. Huang, P. Zhang, Y. Peng, P. Wu, J. Gu, S. Dutkiewicz, H. Zhang, S. Wu, F. Wang, L. Chen, S. Wang and P. Li (2021). Global health effects of future atmospheric mercury emissions. Nature Communications 12(1). http://dx.doi.org/10.1038/s41467-021-23391-7

40 Zhou, T., L. R. Leung, G. Leng, N. Voisin, H. Y. Li, A. P. Craig, T. Tesfa and Y. Mao (2020). Global Irrigation Characteristics and Effects Simulated by Fully Coupled Land Surface, River, and Water Management Models in E3SM. Journal of Advances in Modeling Earth Systems 12(10). http://dx.doi.org/10.1029/2020ms002069

# Method

## Model platform

The MOdel for Scale Adaptive River Transport for Mercury under WateR Management (MOSART-Hg-wrm) is based on the MOSART-Hg model used in an accompanying study (Peng et al. Under Review), with an addition of the water management module integrated into the MOSART-Hg-wrm model (Voisin et al. 2013, Zhou et al. 2020) (Table S3). The model incorporates soil Hg erosion as an input of riverine Hg from natural and legacy sources and considers the contribution of anthropogenic releases. It accounts for the downstream transport of riverine Hg or its settling in riverbeds, while also incorporating the trapping effects of dams on riverine Hg. Implemented within the Community Earth System Model version 2.1.3 (CESM2 version 2.1.3), MOSART-Hg-wrm incorporates features developed from the Energy Exascale Earth System Model (E3SM) (Zhou et al. 2020), including the sediment transport module (Li et al. 2022) and erosion module (Tan et al. 2018, Tan et al. 2022). These modifications enable the simulation of riverine Hg dynamics under contemporary environmental conditions.

The model accounts for water management practices, represented by reservoir constructions globally, allowing the determination of reservoir trap efficiency (Vörösmarty et al. 2003, Voisin et al. 2013, Zhou et al. 2020), albeit without considering reservoir management actions such as storage adjustments. The model facilitates the determination of trapping efficiency by leveraging input datasets of global dams through the calculation method outlined by Vörösmarty et al. (2003). Consequently, the sediment trapping processes can be effectively ascertained. This methodology finds broad application in hydrology and biogeochemical models, exemplified by its utilization in models like Global Nutrient Export from Watersheds 2 (NEWS 2) (Mayorga et al. 2010). Data on global reservoirs are sourced from the Global Reservoir and Dam (GRanD) database (Lehner et al. 2011), initialized on a grid basis by Zhou et al. (2020). This dataset encompasses dam locations, reservoir capacities, and major functions for over 4,200 dams worldwide (Table S3). The trapping efficiency is calculated as followed (Vörösmarty et al. 2003, Li et al. 2022):

$$e_{trap} = 1 - \frac{0.05}{\Delta t_{local}^{0.05}} \quad (1)$$

where $\Delta t_{local}^{0.05}$ is the increase of local water residence time due to the reservoir [years], estimated as the effective reservoir storage capacity divided by the mean annual inflow from the reservoir upstream.

The simulations span the period 1995-2014, with the initial five years dedicated to make the river systems into steady state (i.e., spin-up), and the subsequent five years are considered for analysis. The spatial

resolution matches that of previous studies, with the Community Land Model 5.0 for Mercury (CLM5-Hg) and MOSART-Hg-wrm running at resolutions of 0.9°×1.25° and 0.5°×0.5°, respectively. The former has been extensively evaluated in simulating erosional Hg dynamics (Peng et al. Under Review). We include soil Hg datasets from Wang et al. (Wang et al. 2019) and the Liu et al. (Liu et al. 2023). Climate data, obtained from the GSWP3 dataset, drive the model at a 0.5° horizontal resolution, spanning the same temporal range as previous studies (1995-2014) with a six-hour time resolution. Climate dataset parameters include Precipitation (mm $H_2O$/sec), Incoming Solar Radiation (W/$m^2$), Temperature (K), Pressure (Pa), Winds (m/s), Humidity (kg/kg), and Downward Longwave Radiation (W/$m^2$).

**Anthropogenic Hg release for rivers**

We use an inverse estimation process to establish a plausible range for global Hg releases to rivers. Existing inventories includes that developed by Kocman et al. (2017) (hereafter Kocman inventory), which suggests a global release of Hg to rivers as 1,000 Mg/yr (lower bound). The other inventory is developed by Streets et al. (2017) (hereafter referred to as Streets inventory), which has a global release of Hg to the land and rivers as 7,280 Mg/yr, but the proportion release to land and water are unknown. As only global total releases are provided by these studies, the spatial distribution of Hg sources is based on atmospheric Hg release inventories, namely AMAP inventory (Steenhuisen et al. 2019, Steenhuisen et al. 2022) and Streets Atmospheric inventory (Streets et al. 2019). Indeed, the anthropogenic Hg emissions/releases to atmosphere, land, and water have similar spatial distribution as they share the major contributing sources (Streets et al. 2017). With the MOSART-Hg-wrm model, the Hg release to rivers can be constrained by the global amount of Hg exported to the ocean, ~1,000 Mg/yr based on river monitoring data at river mouths (Liu et al. 2021). Preliminary model simulation indicates that direct driving the MOSART-Hg-wrm with the Kocman inventory generates too low Hg export to the ocean.

The Hg release from sources to rivers are categorized as direct and indirect release. Direct release involves Hg discharge into rivers via urban sewage pipe networks, while indirect release entail Hg initially deposited into the soil, subsequently mobilized by erosional processes, and transported to rivers. The sediment yield serves as a crucial parameter for determining indirect release. In this study, the sediment yield dataset represents the mean sediment yield in 2010, estimated by MOSART-Hg-wrm under the *No Emission scenario*. We also find that altering the portion of direct and indirect release to rivers does not affect the calculated yield.

The grid-based anthropogenic Hg releases to rivers are calculated by the following equations:

$$EI_{ASGM}^{THg} = AMAP_{ASGM}^{THg} \times Sed_{yld} \times Coef_{ASGM}^{I} \quad (2)$$

$$EI_{INDS}^{THg} = AMAP_{INDS}^{THg} \times Sed_{yld} \times Coef_{INDS}^{I} \quad (3)$$

$$EI_{POWERGEN}^{THg} = AMAP_{POWERGEN}^{THg} \times Sed_{yld} \times Coef_{POWERGEN}^{I} \quad (4)$$

where $EI_{ASGM}^{THg}, EI_{INDS}^{THg}, EI_{POWERGEN}^{THg}$ represent the indirect release by ASGM, industrial, or power-generation sectors, respectively (unit: g/km$^2$/yr); $AMAP_{ASGM}^{THg}$, $AMAP_{INDS}^{THg}, AMAP_{POWERGEN}^{THg}$ represent the spatial distribution of release from different sector (unit: g/km$^2$/yr); $Sed_{yld}$ represents the sediment yield (unit: kg/m$^2$/s); and $Coef_{ASGM}^{I}$, $Coef_{INDS}^{I}$, $Coef_{POWERGEN}^{I}$ represent the coefficient of Hg emission associated with erosion (unit: m$^2$s/kg).

$$ED_{ASGM}^{THg} = AMAP_{ASGM}^{THg} \times Coef_{ASGM}^{D} \quad (5)$$

$$ED_{INDS}^{THg} = AMAP_{INDS}^{THg} \times Coef_{INDS}^{D} \quad (6)$$

$$ED_{POWERGEN}^{THg} = AMAP_{POWERGEN}^{THg} \times Coef_{POWERGEN}^{ID} \quad (7)$$

where $ED_{ASGM}^{THg}, ED_{INDS}^{THg}, ED_{POWERGEN}^{THg}$ represent the direct release for varied sectors (unit: g/km$^2$/yr); $AMAP_{ASGM}^{THg}$, $AMAP_{INDS}^{THg}, AMAP_{POWERGEN}^{THg}$ represent the spatial distribution of release (unit: g/km$^2$/yr); and $Coef_{ASGM}^{D}$, $Coef_{INDS}^{D}$, $Coef_{POWERGEN}^{D}$ represent the coefficient of direct Hg emission (taken as unity).

$$E_{total}^{THg} = EI_{ASGM}^{THg} + EI_{INDS}^{THg} + EI_{POWERGEN}^{THg} + ED_{ASGM}^{THg} + ED_{INDS}^{THg} + ED_{POWERGEN}^{THg} \quad (8)$$

where $E_{total}^{THg}$ represents the total anthropogenic Hg release to rivers, which is eventually used to drive the MOSART-Hg-wrm model. The coefficients in equations (2) to (7) are adjustable to suit the requirements of various scenarios, generating a series of scenarios: *Low Emission*, *Moderate Emission*, *High Industrial Emission*, and *High ASGM Emission* with global emission ranging from 1,100 to 2,000 Mg/yr (Table S1).

We find a total anthropogenic emission of ~1,500 Mg/yr best matching the river Hg export to the ocean (*Moderate Emission*). Our estimations suggest that ASGM release account for 30-47% of the total anthropogenic Hg release to rivers (Table S1), which aligns with the assumption of the Kocman inventory that 40% of the release originate from ASGM. To better match the river Hg export dataset, we adopt the spatial pattern of AMAP inventory except for the North America, where the Streets Atmosphere inventory is used, as the former generates too high river Hg export in this region.

**Experiment Design**

The primary experiment (the baseline scenario) conducted in this study employs the *Moderate Emission*

with hybrid spatial distribution suggested by AMAP and Streets Atmosphere inventories. This experiment facilitates a realistic representation of the present-day scenario by closely aligning with observational records. A series of grouped experiments are devised to evaluate uncertainties stemming from different processes: No Reservoir vs. With Reservoir (i.e., driven by *NHHR* and *BHHR*), Inventory (spatial distribution following AMAP or Streets Atmosphere inventories), Soil Hg (soil Hg concentrations following Wang or Liu dataset), and Deposition (no atmospheric deposition or not) (Table S3).

## Uncertainty Analysis

The MOSART-Hg-wrm model has uncertainties comparable to those in previous studies using the MOSART-Hg model (Peng et al. Under Review). We adopt a same model resolution as our previous study focusing on the pre-industrial era (Peng et al. Under Review). We find that the model with a higher resolution (0.5º×0.5º) performs better in simulating erosion flux in single topography units than a coarser resolution (1º×1º), however, the difference can be largely mitigated by using specific scaling factors. To balance computational cost and simulation accuracy, we use a resolution of 0.9º × 1.25º. In general, the accuracy of the erosion processes and riverine sediment/Hg delivery processes are validated against observations in previous studies (Tan et al. 2018, Li et al. 2022). For instance, the model has better performance in simulating global sediment yield compared to alternative models such as the RUSLE model, with a 59% lower discrepancy relative to observations (Tan et al. 2018). Additionally, sediment fluxes in the MOSART-Hg demonstrate similar performance to the BQART model (Peng et al. Under Review).

The water management component (reservoirs/dams) accounts for sediment and riverine Hg trapping effects, alongside their influences on flow processes, which is supported by empirically validated relationships between reservoir properties and river parameters (Vörösmarty et al. 2003) (see Method). The theoretical basin trapping by this method agree well with the observed values, such as the Nile (observed 100% vs. theoretical 99%), Kizil Irmak (observed 98% vs. theoretical 95%) and Krishna River (observed 75% vs. theoretical 70%) (Vörösmarty et al. 2003). The water management module has also been independently validated in previous studies (Zhou et al. 2020, Li et al. 2022). Notably, sediment flux estimations in MOSART-Hg-wrm exhibit high performance compared to previous estimations (Syvitski et al. 2022) (Fig. S2). A similar level of model accuracy is expected for the Hg-trapping effects of reservoirs and dams.

Another source of uncertainties is the spatial distribution of anthropogenic Hg sources to the freshwater

environments. We consider two different atmospheric Hg inventories, AMAP inventory (Steenhuisen et al. 2019, Steenhuisen et al. 2022) and Streets inventory (Streets et al. 2019), as a proxy for the spatial distribution of anthropogenic releases to rivers. The riverine Hg budgets from both scenarios (*AMAP scenario* and *Streets scenario* hereafter) exhibit a strong correlation with observations at a global scale (Fig. S3). However, the different spatial distributions of Hg sources results in varied performances in different regions. The *Streets scenario* shows better performance in simulating riverine Hg in North America, while the *AMAP scenario* performs better in other regions, particularly due to the more detailed sector contributions for the latter.

The soil Hg concentration datasets play a crucial role in the Hg erosion processes. To address the uncertainties stemming from these processes, we conduct the *Soil Hg Experiment* involving different soil Hg concentration datasets (referred to as Liu dataset by Liu et al. (2023) and Wang dataset by Wang et al. (2019)) (see Methods). The diverse datasets exert limited impacts on global-scale riverine Hg budgets, with the Liu dataset resulting in only a slight increase in riverine Hg export to the ocean (<10%) than using Wang dataset. Furthermore, *Deposition Experiment* is devised to assess uncertainties arising from the change of soil Hg concentrations due to atmospheric Hg deposition and the loss of soil Hg by erosion (see Table S3). In this experiment, soil Hg concentrations are dynamically adjusted based on the atmospheric deposition and erosion processes. However, the disparities between the scenarios with constant and dynamic soil Hg concentrations are minimal, with changes in riverine Hg export to the ocean < 2% (Fig. S4). Similarly, given that the rates of gaseous Hg evaporating from rivers are substantially lower than the atmospheric Hg deposition rates (da Silva et al. 2006), the combined uncertainties from gaseous Hg evaporating and deposition are expected to remain within 2%.

## References


1 da Silva, G. S., W. F. Jardim and P. S. Fadini (2006). Elemental gaseous mercury flux at the water/air interface over the Negro River basin, Amazon, Brazil. Science of The Total Environment 368(1): 189-198. http://dx.doi.org/10.1016/j.scitotenv.2005.09.082

2 Kocman, D., S. Wilson, H. Amos, K. Telmer, F. Steenhuisen, E. Sunderland, R. Mason, P. Outridge and M. Horvat (2017). Toward an Assessment of the Global Inventory of Present-Day Mercury Releases to Freshwater Environments. International Journal of Environmental Research and Public Health 14(2): 138. http://dx.doi.org/10.3390/ijerph14020138

3 Lehner, B., C. R. Liermann, C. Revenga, C. Vörösmarty, B. Fekete, P. Crouzet, P. Döll, M. Endejan, K. Frenken, J. Magome, C. Nilsson, J. C. Robertson, R. Rödel, N. Sindorf and D. Wisser (2011). High-resolution mapping of the world's reservoirs and dams for sustainable river-flow management. Frontiers in Ecology and the Environment 9(9): 494-502. http://dx.doi.org/10.1890/100125

4 Li, H.-Y., Z. Tan, H. Ma, Z. Zhu, G. W. Abeshu, S. Zhu, S. Cohen, T. Zhou, D. Xu and L. R. Leung (2022). A new large-scale suspended sediment model and its application over the United States. Hydrology and Earth System Sciences 26(3): 665-688. http://dx.doi.org/10.5194/hess-26-665-2022

5 Liu, Y.-R., L. Guo, Z. Yang, Z. Xu, J. Zhao, S.-H. Wen, M. Delgado-Baquerizo and L. Chen (2023). Multidimensional Drivers of Mercury Distribution in Global Surface Soils: Insights from a Global Standardized Field Survey. Environmental Science & Technology 57(33): 12442-12452. http://dx.doi.org/10.1021/acs.est.3c04313

6 Mayorga, E., S. P. Seitzinger, J. A. Harrison, E. Dumont, A. H. W. Beusen, A. F. Bouwman, B. M. Fekete, C. Kroeze and G. Van Drecht (2010). Global Nutrient Export from WaterSheds 2 (NEWS 2): Model development and implementation. Environmental Modelling & Software 25(7): 837-853. http://dx.doi.org/10.1016/j.envsoft.2010.01.007

7 Peng, D., Z. Tan, T. Yuan, P. Wu, Z. Song, P. Zhang, S. Huang, Y. Zhang, T. Lei, B. A. Middleton, G. Lei and J. Gao (Under Review). Human perturbations to mercury in global rivers.

8 Steenhuisen, F. and S. J. Wilson (2019). Development and application of an updated geospatial distribution model for gridding 2015 global mercury emissions. Atmospheric Environment 211: 138-150. http://dx.doi.org/10.1016/j.atmosenv.2019.05.003

9 Steenhuisen, F. and S. J. Wilson (2022). Geospatially distributed (gridded) global mercury emissions to air from anthropogenic sources in 2015, DataverseNL.

10 Streets, D. G., H. M. Horowitz, D. J. Jacob, Z. Lu, L. Levin, A. F. H. ter Schure and E. M. Sunderland (2017). Total Mercury Released to the Environment by Human Activities. Environmental Science & Technology 51(11): 5969-5977. http://dx.doi.org/10.1021/acs.est.7b00451

11 Streets, D. G., H. M. Horowitz, Z. Lu, L. Levin, C. P. Thackray and E. M. Sunderland (2019). Global and regional trends in mercury emissions and concentrations, 2010–2015. Atmospheric Environment 201: 417-427. http://dx.doi.org/10.1016/j.atmosenv.2018.12.031

12 Syvitski, J., J. R. Ángel, Y. Saito, I. Overeem, C. J. Vörösmarty, H. Wang and D. Olago (2022). Earth's sediment cycle during the Anthropocene. Nature Reviews Earth & Environment 3(3): 179-196. http://dx.doi.org/10.1038/s43017-021-00253-w

13 Tan, Z., L. R. Leung, H. Y. Li and S. Cohen (2022). Representing Global Soil Erosion and Sediment Flux in Earth System Models. Journal of Advances in Modeling Earth Systems 14(1). http://dx.doi.org/10.1029/2021ms002756

14 Tan, Z. L., L. R. Leung, H. Y. Li and T. Tesfa (2018). Modeling Sediment Yield in Land Surface and Earth System Models: Model Comparison, Development, and Evaluation. Journal of Advances in Modeling Earth Systems 10(9): 2192-2213. http://dx.doi.org/10.1029/2017ms001270

15 Voisin, N., H. Li, D. Ward, M. Huang, M. Wigmosta and L. R. Leung (2013). On an improved sub-regional water resources management representation for integration into earth system models. Hydrology and Earth System Sciences 17(9): 3605-3622. http://dx.doi.org/10.5194/hess-17-3605-2013

16 Vörösmarty, C. J., M. Meybeck, B. Fekete, K. Sharma, P. Green and J. P. M. Syvitski (2003). Anthropogenic sediment retention: major global impact from registered river impoundments. Global and Planetary Change 39(1-2): 169-190. http://dx.doi.org/10.1016/s0921-8181(03)00023-7

17 Wang, X., W. Yuan, C.-J. Lin, L. Zhang, H. Zhang and X. Feng (2019). Climate and Vegetation As Primary Drivers for Global Mercury Storage in Surface Soil. Environmental Science & Technology 53(18): 10665-10675.

http://dx.doi.org/10.1021/acs.est.9b02386

18 Zhou, T., L. R. Leung, G. Leng, N. Voisin, H. Y. Li, A. P. Craig, T. Tesfa and Y. Mao (2020). Global Irrigation Characteristics and Effects Simulated by Fully Coupled Land Surface, River, and Water Management Models in E3SM. Journal of Advances in Modeling Earth Systems 12(10). http://dx.doi.org/10.1029/2020ms002069

# Appendix

# Mercury budget in global rivers at present-day: impacts from reservoirs and dams

Dong Peng[1,2], Zeli Tan[3], Peipei Wu[4], Ruirong Chang[2], Shaojian Huang[2], Peng Zhang[2], Yujuan Wang[2], Zhengcheng Song[2], Yanxu Zhang[5], Ting Lei[6], Maodian Liu[7], Jianhua Gao[1], Junguo Liu[8], Guangchun Lei[6], Shu Tao[7,9]

[1]School of Geography and Ocean Science, Ministry of Education Key Laboratory for Coast and Island Development, Nanjing University, Nanjing, China

[2]School of Atmospheric Sciences, Nanjing University, Nanjing, China

[3]Pacific Northwest National Laboratory, Richland, WA, USA

[4]Scripps Institution of Oceanography, University of California San Diego, La Jolla, CA, USA

[5]Department of Earth and Environmental Sciences, Tulane University, New Orleans, LA, USA

[6]School of Ecology and Nature Conservation, Beijing Forestry University, Beijing, China

[7]College of Urban and Environmental Sciences, Peking University, Beijing, China

[8]Henan Provincial Key Laboratory of Hydrosphere and Watershed Water Security, North China University of Water Resources and Electric Power, Zhengzhou, China

[9]School of Environmental Science and Engineering, Southern University of Science and Technology, Shenzhen, China

*Corresponding author: Yanxu Zhang (yzhang127@tulane.edu)

Peer review status:

This is a non-peer-reviewed preprint submitted to EarthArXiv.

# Figures

**Figure S1 Seasonal fluxes of riverine mercury discharge over land**

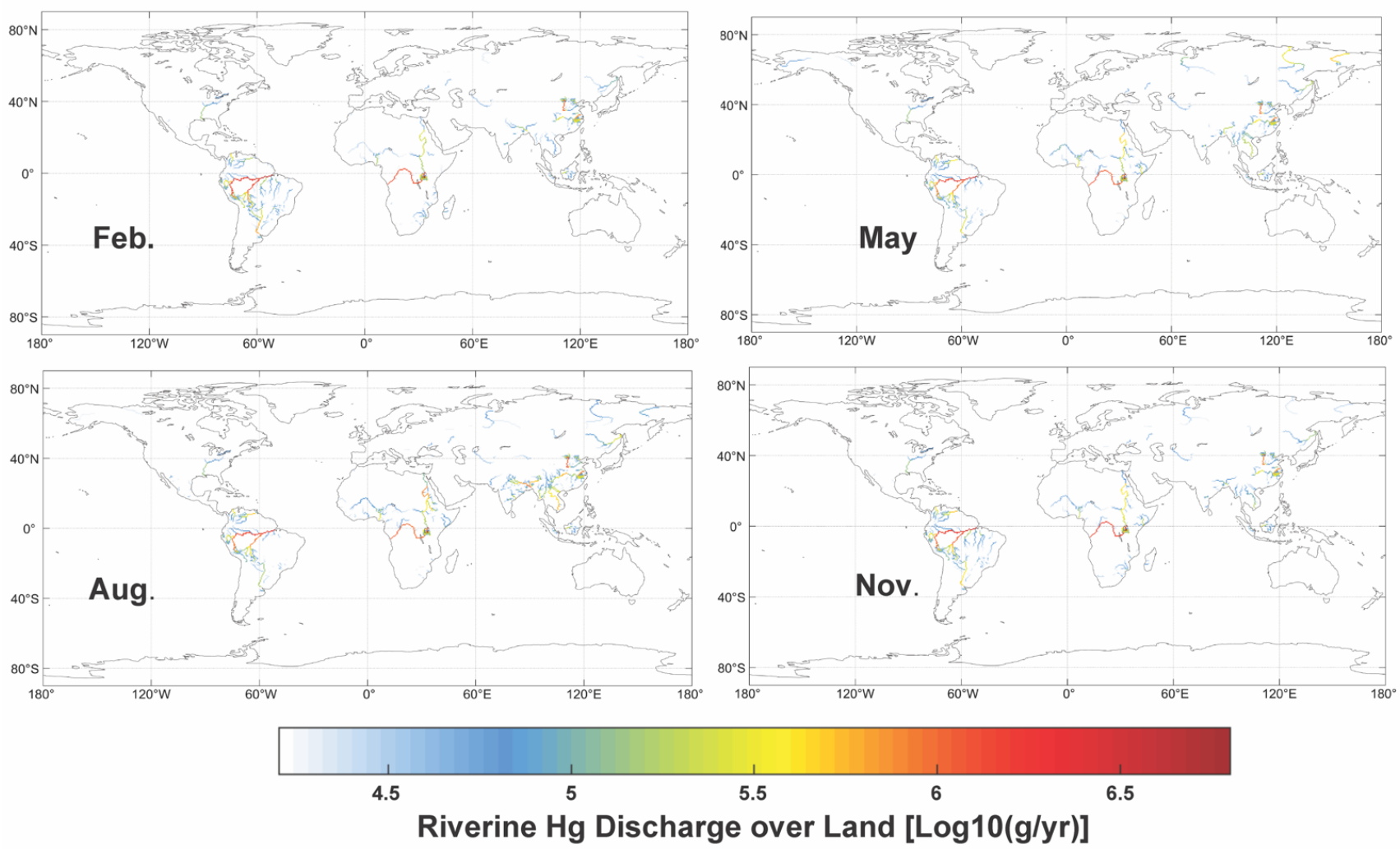

**Figure S2 The sediment load of estimation versus other estimations (Syvitski et al. 2022). The 1950/2010 sediment load is referred to as the estimation by Syvitski et al. (2022).**

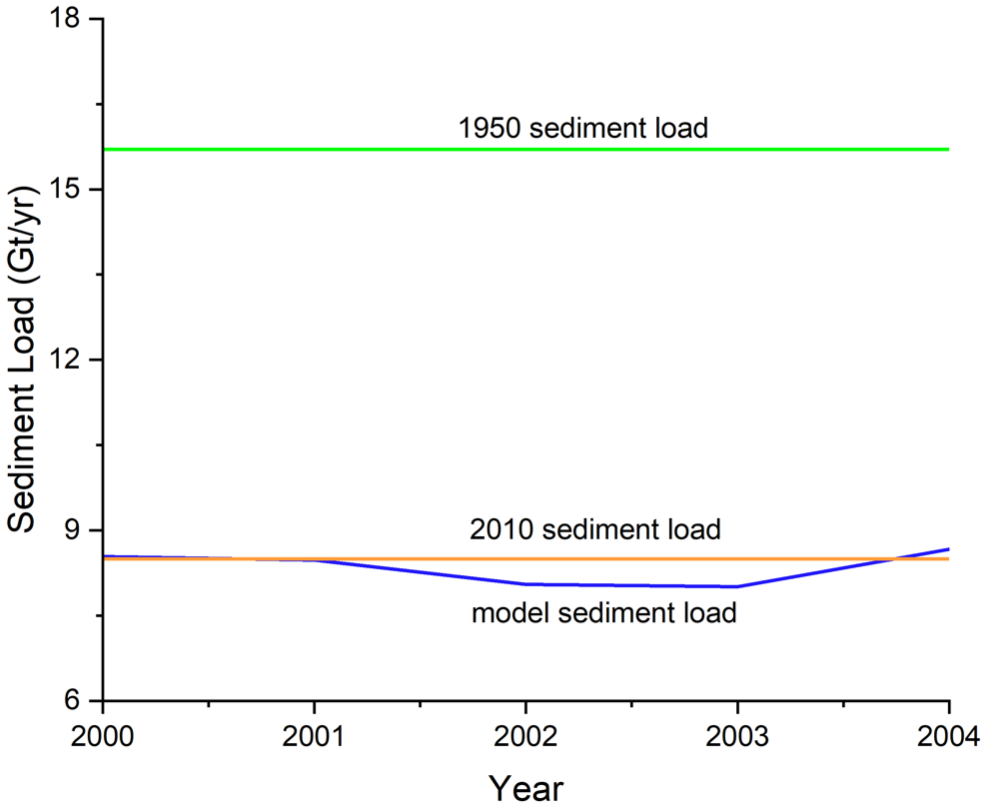

**Figure S3** The comparison of Model results by Inventory Experiment with observation, AMAP represents the AMAP inventory, the Streets represent the Streets inventory (see Table S3).

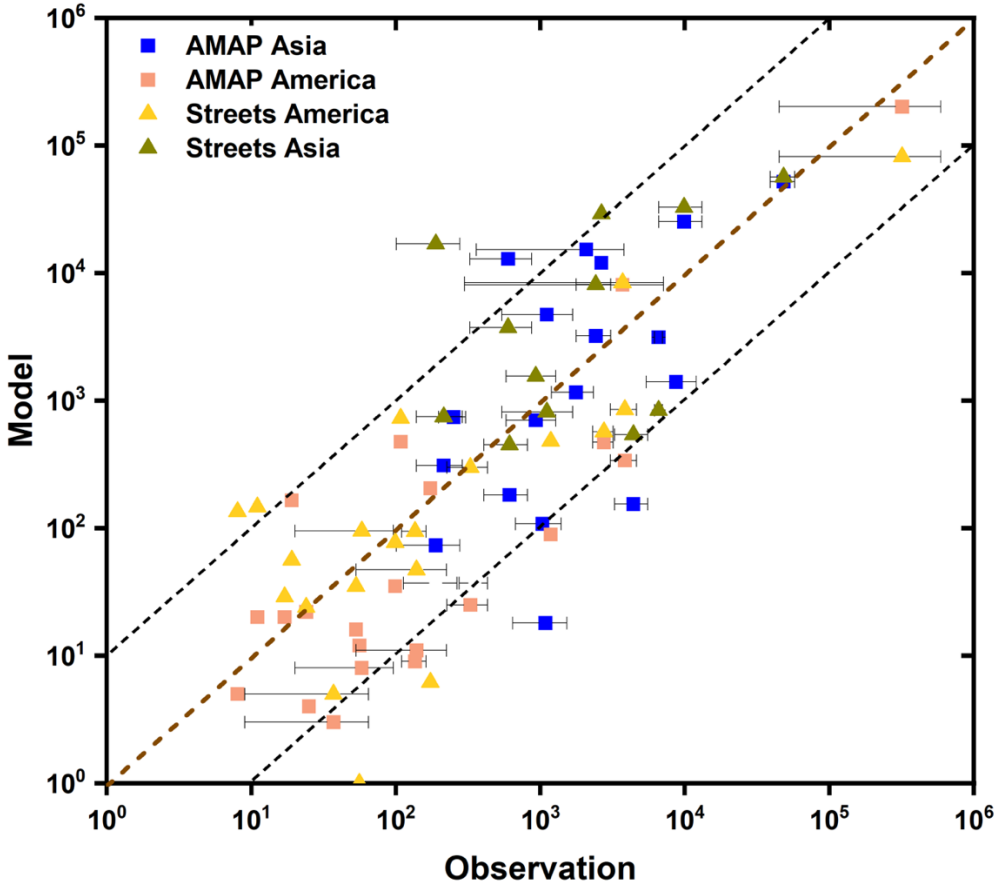

**Figure S4** The comparison of Model results by ***Soil Hg Experiment*** with observation, Wang represents the soil Hg concentration of Wang et al. (2019), the Chen represent the soil Hg concentration dataset of Liu et al. (2023) (see Table S3).

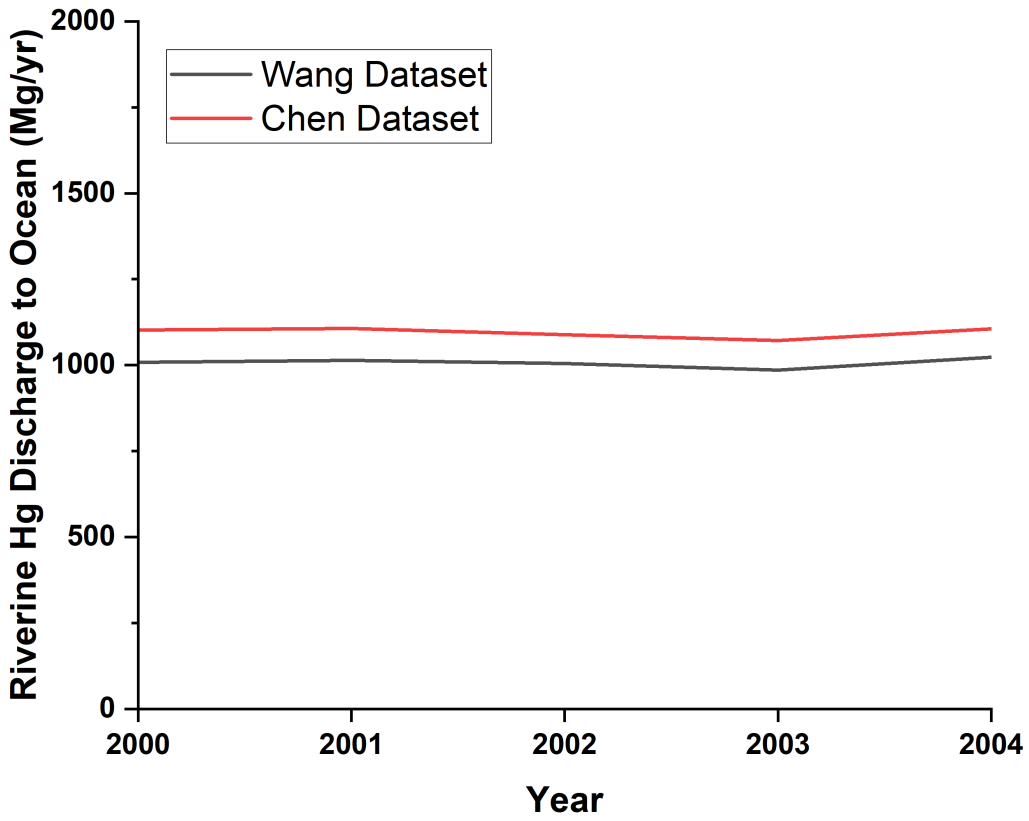

**Figure S5** The comparison of Model results by ***Deposition Experiment*****,** the Deposition represents consider the setting of Deposition in **Table S3**, the Without Deposition represents the setting of Without Deposition in **Table S3**.

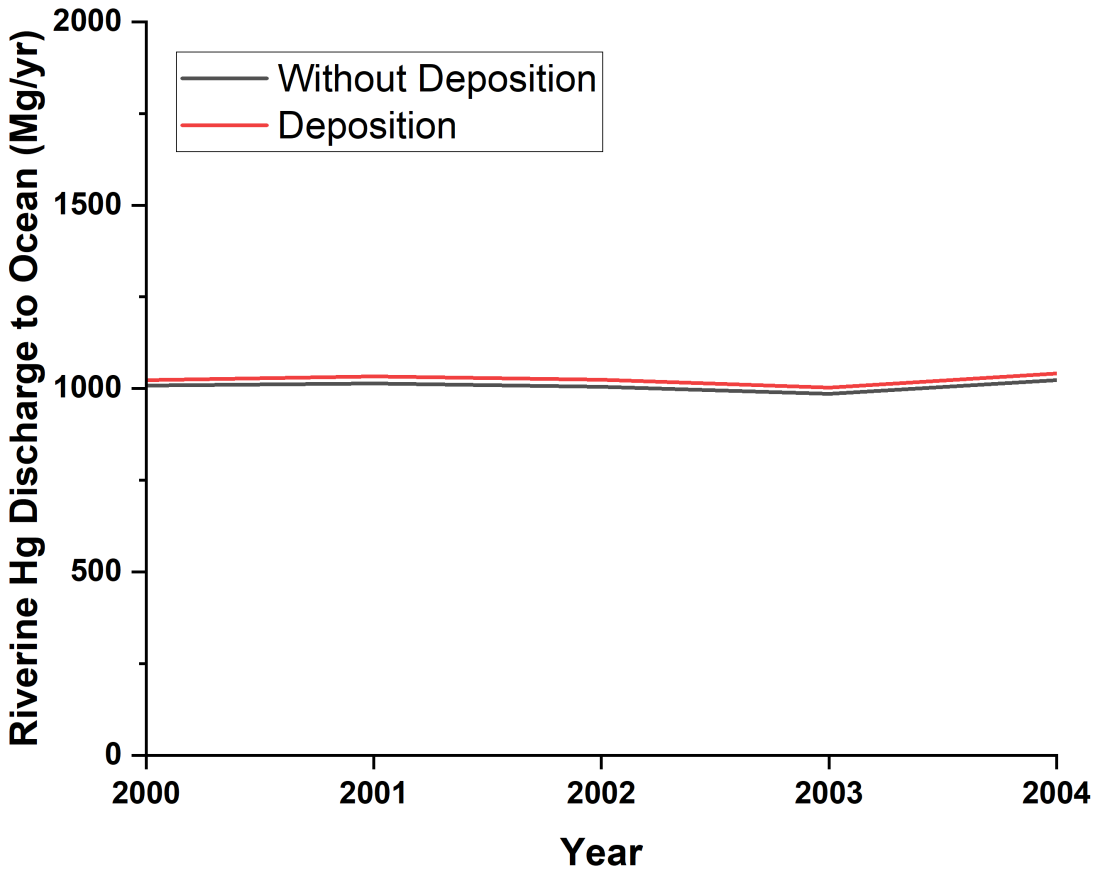

# Tables

**Table S1 The sets of industrial Releases and ASGM Releases.**

| Scenarios | Anthropogenic Hg budget (Mg/yr) | Changes (Mg/yr) | Indirect Release (Mg/yr) | | | Direct Release (Mg/yr) | | |
|---|---|---|---|---|---|---|---|---|
| | | | ASGM | Industrial | | ASGM | Industrial | |
| | | | | INDS | POWERGEN | | INDS | POWERGEN |
| No Release | 0 | = 0 | 0 | 0 | 0 | 0 | 0 | 0 |
| Low Release | 1100 | = No Release + 1100 | 142 | 73 | 8 | 378 | 460 | 39 |
| Moderate Release | 1500 | = Low Release + 400 | 232 | 84 | 6 | 378 | 748 | 59 |
| Revised AMAP Release | About 1500 | | | ≈ Moderate Release | | | | |
| High Industrial Release | 2000 | = Moderate Release + 500 | 232 | 343 | 25 | 378 | 949 | 74 |
| High ASGM Release | 2000 | = Moderate Release + 500 | 367 | 132 | 9 | 475 | 949 | 74 |

**Table S2 Fates of Riverine mercury under different scenarios.**

| Scenarios | Anthropogenic Hg Releases (Mg/yr) | Inputs of Riverine Hg (Mg/yr) | Outputs of Riverine Hg (Mg/yr) | Increased Release* (Mg/yr) | Increased Outputs (Mg/yr) | Increased Export/ Increased Releases (%) |
|---|---|---|---|---|---|---|
| No | 0 | 418 | 248 | 0 | - | - |
| Low | 1100 | 1498 | 777 | 1100 | 529 | 48% |
| Moderate | 1500 | 2005 | 1007 | 400 | 230 | 58% |
| High Industrial | 2000 | 2532 | 1146 | 500 | 139 | 28% |
| High ASGM | 2000 | 2436 | 1275 | 500 | 268 | 54% |

Caption: * the increased Release as compared with the previous one, such as ‘moderate – low = 400’, ‘high -moderate=500’.

**Table S3 Experiments Design.**

| Experiment ID | Experiment Name | Soil Hg Concentration Dataset | Anthropogenic Hg Release (Mg/yr) | Soil Hg Dynamic | Atmospheric Hg Deposition | Water Management | Spatial Distribution of Release | Release Scenario |
|---|---|---|---|---|---|---|---|---|
| **Baseline** | | Wang | About 1500 | Constant | No | Yes | AMAP2015 | Revised AMAP |
| **Anthropogenic Release Uncertainty** | | | 0 | | | | | No |
| | | | 1100 | | | | | Low |
| | | | 1500 | | | | | Moderate |
| | | | 2000 | | | | | High ASGM |
| | | | 2000 | | | | | High Industrial |
| **Water Management** | No Release without wrm | | 0 | | | No | | No |
| | No Release with wrm | | | | | Yes | | |
| | Baseline without wrm | | 1500 | | | No | | Revised AMAP |
| | Baseline with wrm | | | | | Yes | | |
| **Inventory** | AMAP | | | | | Yes | AMAP 2015 | Moderate |
| | Streets | | | | | | Streets | |
| **Soil Hg** | Wang | Wang | | | | | AMAP 2015 | |
| | Chen | Chen | | | | | | |
| **Deposition** | Deposition | Wang | | Dynamic | Yes | | | |
| | Without Deposition | | | Constant | No | | | |

Caption: Wang represents the soil Hg dataset from Wang et al. (2019), Chen represents the soil Hg concentration from Liu et al. (2023), AMAP2015 represents the inventory by Steenhuisen et al. (2019), Steenhuisen et al. (2022), Streets represents the inventory of Streets et al. (2019).

# References


1 Liu, Y.-R., L. Guo, Z. Yang, Z. Xu, J. Zhao, S.-H. Wen, M. Delgado-Baquerizo and L. Chen (2023). Multidimensional Drivers of Mercury Distribution in Global Surface Soils: Insights from a Global Standardized Field Survey. Environmental Science & Technology 57(33): 12442-12452. http://dx.doi.org/10.1021/acs.est.3c04313

2 Steenhuisen, F. and S. J. Wilson (2019). Development and application of an updated geospatial distribution model for gridding 2015 global mercury emissions. Atmospheric Environment 211: 138-150. http://dx.doi.org/10.1016/j.atmosenv.2019.05.003

3 Steenhuisen, F. and S. J. Wilson (2022). Geospatially distributed (gridded) global mercury emissions to air from anthropogenic sources in 2015, DataverseNL.

4 Streets, D. G., H. M. Horowitz, Z. Lu, L. Levin, C. P. Thackray and E. M. Sunderland (2019). Global and regional trends in mercury emissions and concentrations, 2010–2015. Atmospheric Environment 201: 417-427. http://dx.doi.org/10.1016/j.atmosenv.2018.12.031

5 Syvitski, J., J. R. Ángel, Y. Saito, I. Overeem, C. J. Vörösmarty, H. Wang and D. Olago (2022). Earth's sediment cycle during the Anthropocene. Nature Reviews Earth & Environment 3(3): 179-196. http://dx.doi.org/10.1038/s43017-021-00253-w

6 Wang, X., W. Yuan, C.-J. Lin, L. Zhang, H. Zhang and X. Feng (2019). Climate and Vegetation As Primary Drivers for Global Mercury Storage in Surface Soil. Environmental Science & Technology 53(18): 10665-10675. http://dx.doi.org/10.1021/acs.est.9b02386